3′-Deoxy-3′-[18F]Fluorothymidine as a New Marker for Monitoring Tumor Response to Antiproliferative Therapy *in Vivo* with Positron Emission Tomography[1]

Henryk Barthel, Marcel C. Cleij, David R. Collingridge, O. Clyde Hutchinson, Safiye Osman, Qimin He, Sajinder K. Luthra, Frank Brady, Pat M. Price, and Eric O. Aboagye[2]

Cancer Research United Kingdom PET Oncology Group, Department of Cancer Medicine, Faculty of Medicine, Imperial College of Science, Technology and Medicine, Hammersmith Hospital Campus, London W12 0NN, United Kingdom [H. B., M. C. C., D. R. C., O. C. H., P. M. P., E. O. A.]; Imaging Research Solutions Limited, Cyclotron Building, Hammersmith Hospital, London W12 0NN, United Kingdom [S. O., S. K. L., F. B.]; Department of Nuclear Medicine, University of Leipzig, 04103 Leipzig, Germany [H. B.]; and Department of Oncology, Clinical Research Laboratory, Huddinge University Hospital, Karolinska Institute, S-171 76 Stockholm, Sweden [Q. H.]

ABSTRACT

3′-Deoxy-3′-[18F]fluorothymidine ([18F]FLT) has been proposed as a new marker for imaging tumor proliferation by positron emission tomography (PET). The uptake of [18F]FLT is regulated by cytosolic S-phase-specific thymidine kinase 1 (TK1). In this article, we have investigated the use of [18F]FLT to monitor the response of tumors to antiproliferative treatment *in vivo*. C3H/Hej mice bearing the radiation-induced fibrosarcoma 1 tumor were treated with 5-fluorouracil (5-FU; 165 mg/kg i.p.). Changes in tumor volume and biodistribution of [18F]FLT and 2-[18F]fluoro-2-deoxy-D-glucose ([18F]FDG) were measured in three groups of mice ($n = 8$–12/group): (*a*) untreated controls; (*b*) 24 h after 5-FU; and (*c*) 48 h after 5-FU. In addition, dynamic [18F]FLT-PET imaging was performed on a small animal scanner for 60 min. The metabolism of [18F]FLT in tumor, plasma, liver, and urine was determined chromatographically. Proliferation was determined by staining histological sections for proliferating cell nuclear antigen (PCNA). Tumor levels of TK1 protein and cofactor (ATP) were determined by Western blotting and bioluminescence, respectively. Tumor [18F]FLT uptake decreased after 5-FU treatment (47.8 ± 7.0 and $27.1 \pm 3.7\%$ for groups *b* and *c*, respectively, compared with group *a*; $P < 0.001$). The drug-induced reduction in tumor [18F]FLT uptake was significantly more pronounced than that of [18F]FDG. The PET image data confirmed lower tumor [18F]FLT retention in group *c* compared with group *a*, despite a trend toward higher radiotracer delivery for group *c*. Other than phosphorylation in tumors, [18F]FLT was found to be metabolically stable *in vivo*. The decrease in tumor [18F]FLT uptake correlated with the PCNA-labeling index ($r = 0.71$, $P = 0.031$) and tumor volume changes after 5-FU treatment ($r = 0.58$, $P = 0.001$). In this model system, the decrease in [18F]FLT uptake could be explained by changes in catalytic activity but not translation of TK1 protein. Compared with group *a*, TK1 levels were lower in group *b* ($78.2 \pm 5.2\%$) but higher in group *c* ($141.3 \pm 9.1\%$, $P < 0.001$). In contrast, a stepwise decrease in ATP levels was observed from group *a* to *b* to *c* ($P < 0.001$). In conclusion, we have demonstrated the ability to measure tumor response to antiproliferative treatment with [18F]FLT and PET. In our model system, the radiotracer uptake was correlated with PCNA-labeling index. The decrease in [18F]FLT uptake after 5-FU was more pronounced than that of [18F]FDG. [18F]FLT is, therefore, a promising marker for monitoring antiproliferative drug activity in oncology that warrants additional testing.

INTRODUCTION

Current knowledge in tumor biology is providing new opportunities for cancer treatment. Of particular interest are molecules, which interfere with growth signal transduction, cell cycle control, differentiation, apoptosis, and angiogenesis (1–3). For early proof of principle trials in humans, pharmacodynamic endpoints for these new drugs need to be defined. Noninvasive imaging techniques are particularly attractive for this purpose. To date, tumor shrinkage as measured by ultrasound, X-ray transmission computed tomography, or magnetic resonance imaging still constitutes the mainstay of assessing tumor response to treatment (4, 5). Other than the fact that necrosis, scar tissue formation, and inflammation can confound the anatomical detection of therapy response, several of the novel therapies are cytostatic and do not implicitly lead to a decrease of the tumor volume (5). In addition, tumor volume changes may occur only after weeks or months after therapy, impeding quick decisions on therapy modification in the case of nonresponse.

These drawbacks could be overcome by using functional imaging techniques like PET.[3] PET with [11C]dThd has been shown to be suitable for imaging tumor proliferation and response to cancer therapies in the clinic (6–11). Because of the rapid *in vivo* degradation of [11C]dThd, however, investigators have sought analogues that are less readily metabolized (12, 13). A promising candidate is [18F]FLT, the radiolabeled form of a pyrimidine nucleoside that was first described in 1969 by Langen *et al.* (14–16) as a selective inhibitor of DNA synthesis. After permeating the cell membrane by a carrier-mediated mechanism, as well as by passive diffusion (17), FLT undergoes monophosphorylation catalyzed by cytosolic TK1 enzyme. This implies that the [18F]FLT signal detected by PET presumably gives a measure of the TK1 activity. This presumption has recently been supported by *in vitro* experiments in A549 human lung carcinoma cells, where a positive correlation between [18F]FLT uptake by cells and TK1 activity was seen (18). Because TK1 activity correlates with the degree of cellular proliferation (19) and shows a (complex) S-phase-regulated expression (20, 21), it has been suggested that imaging this surrogate marker will provide a reasonable measure of tumor proliferation (12).

FLT labeled with 18F was firstly described in 1991 by Wilson *et al.* (22) as carrier-added [18F]FLT and in 1997 by Grierson *et al.* (23) as no-carrier-added [18F]FLT. Over the last few years, different approaches to increase the radiochemical yield of the radiotracer have been published [for overview see Mier *et al.* (24)]. In 1998, [18F]FLT was firstly applied for PET imaging. Shields *et al.* (12) investigated

animals and a non-small cell lung cancer patient and found [18F]FLT to be specifically taken up into proliferating tissues, including tumors and bone marrow. Recently, Buck *et al.* (25) performed [18F]FLT-PET studies in 30 patients with solitary pulmonary nodules. In this primary diagnostic imaging study, a positive correlation between tumor radiotracer uptake and proliferative activity, as measured histologically by Ki-67 immunostaining, was demonstrated (25).

There are, however, no investigations reported to date on the use of [18F]FLT for imaging tumor response to therapy. The present study was, therefore, initiated to assess [18F]FLT for therapy monitoring with PET in a model system for which the response profile is well known, *i.e.,* RIF-1 xenografts treated with 5-FU (26, 27). In addition, this study was carried out with the view to provide clarity on the uptake mechanism of [18F]FLT in proliferating tumors and, in particular, on the role of TK1 and cofactor (ATP) for realizing TK1 activity. Furthermore, we have compared [18F]FLT uptake to that of [18F]FDG, the current standard for therapy monitoring in oncology by PET.

MATERIALS AND METHODS

Radiopharmaceuticals. [18F]FLT and [18F]FDG were produced on-site by Imaging Research Solution Limited (MRC Cyclotron Building, Hammersmith Hospital, London, United Kingdom). [18F]FLT was prepared by radiofluoridation of the 2,3′-anhydro-5′-*O*-(4,4′-dimethoxytrityl)-thymidine precursor using an improved synthesis system that was recently developed in our institute (28), with a radiochemical yield of 32%. [18F]FDG was produced by a stereospecific nucleophilic fluorination reaction followed by deprotection to obtain a no-carrier-added product as reported previously (29). The range of specific radioactivities of [18F]FLT and [18F]FDG were 46.5–80.8 and 19.6–722.0 $GBq.\mu mol^{-1}$, respectively.

Animals and Tumor Models. The experiments were performed by licensed investigators in accordance with the United Kingdom Home Office's "Guidance on the Operation of the Animal (Scientific Procedures) Act 1986." Ten to 12-week-old male C3H/Hej mice were obtained from Harlan United Kingdom Ltd. (Bicester, United Kingdom). RIF-1 tumor xenografts were established s.c. on the back of the mice by injecting 5×10^5 cells in 100 μl of Dulbecco's PBS. From the first visualization of the tumors up to the day of the final experiments, tumor dimensions were measured continuously using a caliper. Tumor volumes were calculated using the equation: volume = $(\pi/6) \times a \times b \times c$, where *a*, *b*, and *c* represent three orthogonal axes of the tumor. The treatment experiments were started 14–18 days after implantation, when the tumors reached a volume of ~100 mm^3.

5-FU Treatment. The 5-FU solution for injection was obtained from Faulding Pharmaceuticals (Queensway, United Kingdom) and administered as a single bolus injection at a dose of 165 mg/kg 5-FU i.p. The injections were performed 24 or 48 h before the radiotracer experiments. Untreated RIF-1 tumor-bearing mice served as controls.

Immunohistochemical Examination of RIF-1 Tumors. For histological evaluation of the degree of tumor proliferation, untreated ($n = 3$) and 5-FU-treated tumors [24 h ($n = 4$) and 48 h ($n = 4$) posttreatment] were excised, fixed in formalin, embedded in paraffin, and cut into 5.0-μm sections. Adjacent sections were stained with H&E or mouse monoclonal antibodies for PCNA (Novocastra, Newcastle-upon-Tyne, United Kingdom). The primary PCNA antibodies were subsequently detected with biotinylated goat antimouse IgG antibodies (Dako, Carpinteria, CA) and peroxidase-labeled streptavidin (Roche Diagnostics, Lewes, United Kingdom). Peroxidase-labeled cells were visualized by incubation with hydrogen peroxide and diaminobenzidine tetrahydrochloride (Chromogen; Sigma, Poole, United Kingdom). Sections from two different regions of each tumor, separated by at least 1.0 mm, were used for the analyses. The numbers of PCNA- and H&E-positive cells in adjacent sections were counted in five randomly selected fields of view (0.37 mm^2) per section using a BX51 Olympus microscope (Olympus Optical, Tokyo, Japan) at $\times 600$ magnification. The LI_{PCNA} was calculated using the equation $LI_{PCNA} = (cells_{PCNA-positive}/cells_{H\&E-positive}) \times 100\%$.

Western Blot Analysis of TK1(Protein) Levels in RIF-1 Tumors. RIF-1 tumors, untreated controls and 5-FU-treated, were excised and immediately

frozen in liquid nitrogen. Tumor samples were pulverized with the aid of liquid nitrogen and homogenized in ice-cold Dulbecco's PBS. Samples were then centrifuged (2790 rpm for 30 min at 4°C) to obtain the supernatant. The resulting supernatants were taken for additional analysis. The protein content of the supernatants was determined using a commercial kit (BCA protein assay kit; Pierce, Rockford, IL).

TK1 protein levels were determined by Western blot as previously reported by He *et al.* (30, 31). Briefly, aliquots of the tumor samples (containing 30 μg of protein) were mixed with equivalent volumes of native Tris-glycine sample buffer (Novex; Invitrogen, Groningen, the Netherlands) and separated on precast Tris-glycine (4–20%) gel (ICN Biomedicals, Aurora, OH). Electrophoresis was performed at a constant current of 12 mA. The separated proteins were transferred onto a nitrocellulose membrane (Hybond ECL; Amersham Pharmacia Biotech, Little Chalfont, United Kingdom) and subsequently blocked with TBS/casein-blocking buffer [20 mM Tris, 0.5 M NaCl, 1% casein (pH 7.4); Bio-Rad Laboratories, Hercules, CA]. TK1 was detected with mouse antibodies (monoclonal antibody no. 1D11) raised against a synthetic peptide (amino acids K211PGEAVAARKLFAPQ255) that corresponds to a part of the COOH-terminus of rodent and human TK1 (Svanova Biotech, Uppsala, Sweden). The nitrocellulose membrane was incubated with anti-TK1 monoclonal antibody [initial concentration 1 mg/ml; 1:25,000 dilution in TBS-T buffer (20 mM Tris, 150 mM NaCl, and Tween 20 0.1% v/v)] for at least 15 h, washed with TBS-T, and incubated for 60 min with antimouse IgG horseradish peroxidase (Santa Cruz Biotechnology, Santa Cruz, CA) at a dilution of 1:15,000 TBS-T buffer. The membrane was washed again and visualized using the enhanced chemiluminescence method (SuperSignal West Pico Chemiluminescent Substrate; Pierce). For quantification of band intensities, the films were scanned using a GS-710 Calibrated Imaging Densitometer (Bio-Rad Laboratories) and analyzed with the Quantity One software (version 4.0.3; Bio-Rad Laboratories). The molecular weight of the detected bands was estimated from molecular weight marker (Kaleidoscope Prestained Standards; Bio-Rad Laboratories) bands, which were blotted in parallel with the original samples. The tumor samples were analyzed in triplicate/native gel, and the analysis was repeated twice. The complete experiment (including establishment of tumor xenografts, 5-FU treatment, harvesting of the tumors, and preparation of samples for native electrophoresis) was repeated three times.

Determination of ATP Levels in RIF-1 Tumors. ATP levels in the RIF-1 tumors were determined by a bioluminescence assay (ENLITEN ATP assay system; Promega Corporation, Madison, WI). The assay measures the ATP-dependent emission of light at 560 nm from a luciferase/luciferin reaction. Light intensity, which is proportional to the ATP concentration, was measured using a microplate luminescence counter (TopCount NXT; Packard Instrument, Meriden, CT). Supernatants prepared as described for Western blot analysis were analyzed for ATP levels and normalized to the total cellular protein levels determined by the BCA protein assay kit (Pierce). A calibration curve was prepared from ATP standards, which were provided with the above ATP assay kit.

[18F]FLT and [18F]FDG Biodistribution Studies. Untreated and 5-FU-treated RIF-1-tumor-bearing mice were administered a bolus injection of [18F]FLT or [18F]FDG i.v. via the lateral tail vein at a dose of 60–80 μCi (2.22–2.96 MBq). The mice were sacrificed 60 min after radiotracer injection by exsanguination via cardiac puncture (under general isofluorane inhalation anesthesia). Blood, normal tissues (liver, kidneys, lung, brain, spinal cord, spleen, heart, leg muscle, leg bone, and small intestine), as well as tumor samples were rapidly excised. In addition, urine was collected, and plasma was obtained from blood centrifugation. All samples were weighed, and the radioactivity was measured using a Cobra II Auto-Gamma counter (Packard Instrument), applying a decay correction. The results were expressed as %ID/g.

[18F]FLT Metabolite Analyses. In parallel with the *ex vivo* biodistribution studies, plasma, urine, liver and tumor samples were assessed for putative [18F]FLT metabolites by reversed-phase HPLC. Plasma samples were deproteinated by adding ice-cold acetonitrile (2 × volumes) and centrifuged (3000 × g, 5 min, 4°C). Liver and tumor samples were cut into small pieces and homogenized with two parts of ice-cold acetonitrile using an Ultra-Thurrax homogenizer (IKA, Staufen, Germany) and the resultant homogenate centrifuged (3000 × g, 5 min, 4°C). The supernatant from plasma and tissues were evaporated to dryness in a rotary evaporator (40°C) under vacuum, reconstituted in 1.5 ml of mobile phase and filtered (0.2 μm). Unlike plasma and tissue samples, urine samples were diluted with 1.5 ml of mobile phase and

3792

clarified by filtration (0.2 μm). Aliquots of each filtrate (plasma, tumor, liver, and urine; 1 ml) were injected into the HPLC system. Samples were separated on a C$_{18}$ μBondapak column (7.8 × 300 mm, size 10 μm; Waters, Milford, MA) that was eluted with 0.1 M KH$_2$PO$_4$/acetonitrile (85/15% v/v; pH 4.5) at a flow rate of 3.0 ml/min. The radioactivity of the eluents was monitored. Peak areas were integrated and corrected for physical decay and background activity.

Biochemical evidence that the tumor metabolite of [^{18}F]FLT was a 5′-phosphate was provided by incubating tumor homogenates (for 60 min at 37°C) with 5 mM Tris-HCl buffer solution (pH 7.4) containing 50% (v/v) glycerol, 0.5 mM MgCl, 0.5 mM ZnCl$_2$, and 10 units of bacterial (type III) alkaline phosphatase (Sigma). The reaction was terminated by adding ice-cold acetonitrile, and the samples were kept on ice before analysis. Samples were clarified as above and analyzed by HPLC. Control experiments were performed without alkaline phosphatase.

PET Imaging and Image Analysis. Toward PET imaging in humans, we investigated the biodistribution of [^{18}F]FLT *in vivo* by PET scanning on a second generation-dedicated small animal PET scanner, quad-HIDAC [Oxford Positron Systems, Weston-on-the-Green, United Kingdom (32)]. The 32-module quad-HIDAC has the following features: 17- and 28-cm field of view in the transaxial and axial planes, respectively; 1.0 and 1.5 mm spatial resolution (full-width half-maximum) in both planes at 0.125- and 0.5-mm sinogram bin size, respectively; and 1.2% scatter corrected efficiency on a line source with no energy discrimination. Each of three untreated and three tumor-bearing mice treated with 5-FU 48 h before the experiment were scanned. For this, the tail veins of the mice were cannulated after induction of anesthesia with isofluorane/O$_2$/N$_2$O. The animals were placed within a thermostatically controlled jig and positioned prone in the scanner. The jig has been calibrated to provide a rectal temperature of 37°C. A bolus injection of 80 μCi (2.96 MBq) [^{18}F]FLT was administered via the tail cannula and scanning commenced. Dynamic emission scans were acquired in list mode format over 60 min. The acquired data were sorted into 0.5-mm sinogram bins and 19 time frames (4 × 15 s, 4 × 60 s, and 11 × 300 s) for image reconstruction, which was performed by filtered back projection using a two-dimensional Hamming filter (cutoff 0.6). The image data sets obtained were transferred to a SUN workstation (Ultra 10; SUN Microsystems, Santa Clara, CA) and visualized using the Analyze software (version 4.0; Biomedical Imaging Resource, Mayo Clinic, Rochester, MN). ROIs were defined on three to six coronal planes for all tumors. TACs from the ROIs were averaged for each tumor and normalized to the injected activity.

Statistical Analysis. Statistical analyses were performed using the software SPSS for Windows, version 10.0.7 (SPSS, Inc., Chicago, IL). Differences between control and 5-FU-treated groups with respect to tumor volume changes, LI$_{PCNA}$, TK1 protein levels, ATP levels, as well as [^{18}F]FLT and [^{18}F]FDG tumor uptake were tested for significance using one-factorial ANOVA. Differences between the [^{18}F]FLT and [^{18}F]FDG biodistribution and the [^{18}F]FLT-PET imaging data of 5-FU-treated and untreated tumor-bearing mice were tested for significance using the two-sided Student' *t* test for independent samples. Correlations between the radiotracer uptake into tumors and tumor volume changes, as well as between [^{18}F]FLT tumor uptake and LI$_{PCNA}$ were determined by linear regression analyses. Unless stated, data were mean ± 1 SE. *P*s of ≤0.05 were considered significant.

RESULTS

5-FU Is Cytotoxic to RIF-1 Tumors. The biological activity of 5-FU on tumors was assessed by measuring changes in tumor volume
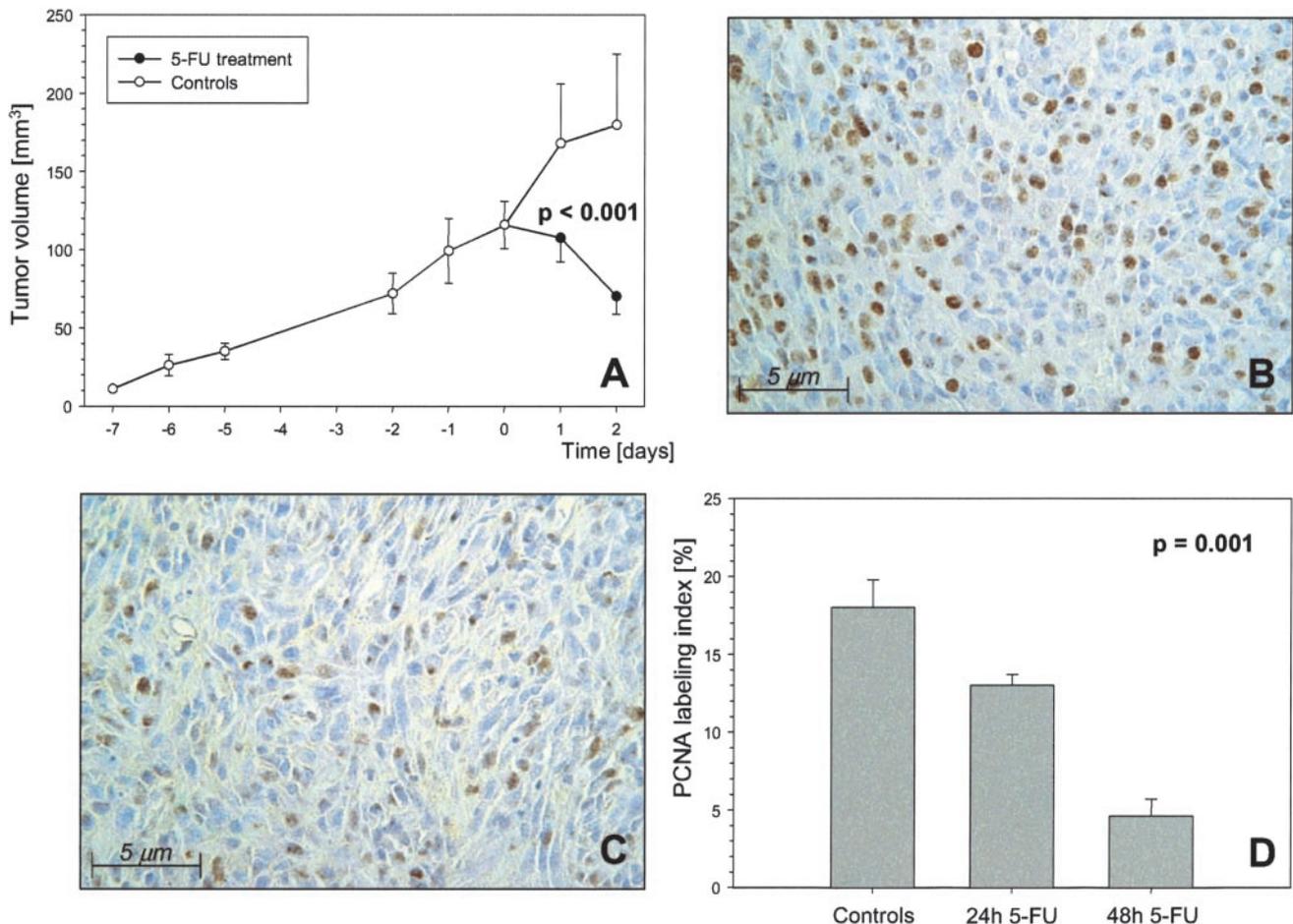

Fig. 1. 5-FU treatment and tumor proliferation. Effect of 5-FU (165 mg/kg i.p.) on proliferation of RIF-1 tumors. *A*, changes in tumor volume. 5-FU was injected on day 0 (*n* = 8 mice/group). *B*, typical PCNA-stained histological section of an untreated RIF-1 tumor. *C*, typical PCNA-stained histological section of a RIF-1 tumor 48 h after 5-FU treatment. *D*, changes in ^{LI}PCNA in untreated and 5-FU-treated tumors (24 and 48 h after treatment). The differences in *brown staining* in *B* and *C* reflect differences in proliferation.
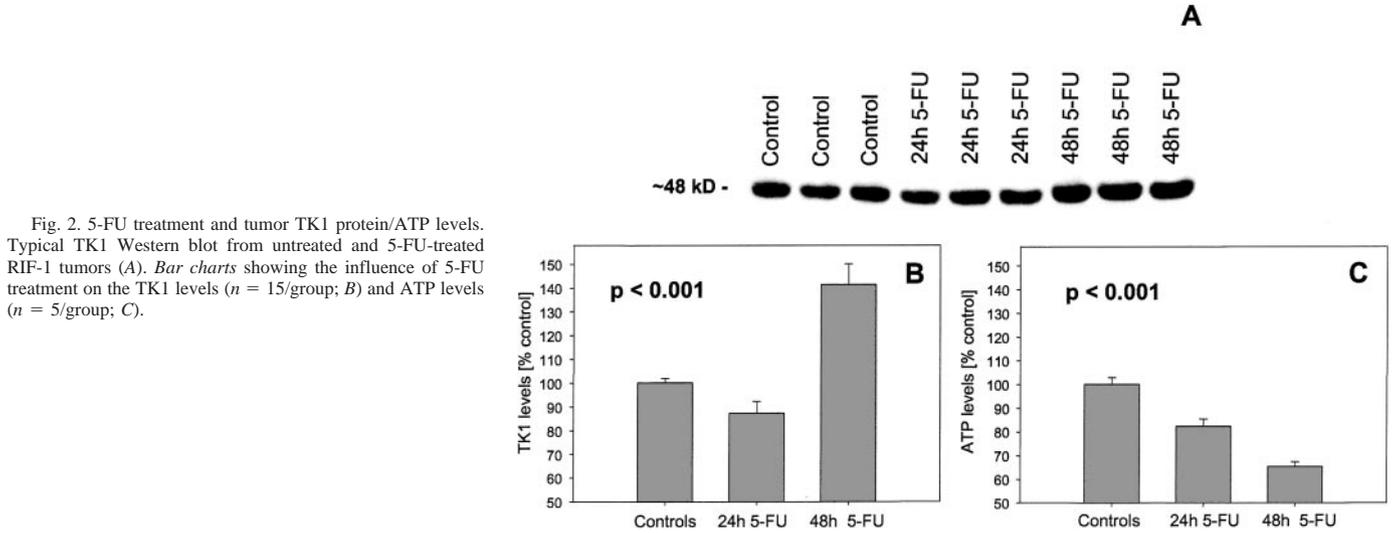
3793

Fig. 2. 5-FU treatment and tumor TK1 protein/ATP levels. Typical TK1 Western blot from untreated and 5-FU-treated RIF-1 tumors (*A*). *Bar charts* showing the influence of 5-FU treatment on the TK1 levels ($n = 15$/group; *B*) and ATP levels ($n = 5$/group; *C*).

and LI_{PCNA}. Fig. 1*A* shows the growth characteristics of RIF-1 tumors and the effect of 5-FU ($n = 8$ mice/group). Untreated mice showed a volume increase of $52.6 \pm 29.1\%$ compared with the tumor size on the day of treatment. In contrast, 5-FU treatment resulted in tumor shrinkage. Tumor volumes decreased in this group by 25.6 ± 19.7 and $33.5 \pm 14.6\%$ at 24 and 48 h, respectively, after treatment compared with pretreatment tumors ($P < 0.001$, one-factorial ANOVA).

PCNA-stained histological sections of untreated and 5-FU-treated (48 h after treatment) RIF-1 tumors are shown in Fig. 1, *B* and *C*, respectively. In keeping with the decrease in tumor volume, there was a stepwise decrease in LI_{PCNA} after 5-FU treatment (Fig. 1*D*). LI_{PCNA} decreased by 27.5 ± 1.5 and $74.2 \pm 17.2\%$ at 24 and 48 h after treatment, respectively, compared with pretreatment LI_{PCNA} ($P = 0.001$, one-factorial ANOVA).

5-FU Treatment Alters Tumor TK1 Enzyme and ATP Levels. TK1 activity has been proposed as the most important determinant of [18F]FLT uptake. Thus, we investigated the effect of 5-FU on tumor TK1 protein levels and cofactor (ATP) levels. Western blots of TK1 protein from untreated and 5-FU-treated tumors (24 and 48 h after treatment) are shown in Fig. 2*A*. Analysis of band intensities by densitometry at 24 h after treatment showed a $12.8 \pm 0.8\%$ reduction in TK1 protein levels compared with control levels (Fig. 2*B*). Unexpectedly, TK1 protein levels were higher than that of controls at 48 h after treatment (a $41.3 \pm 2.6\%$ increase, $P < 0.001$, one-factorial ANOVA; Fig. 2*B*).

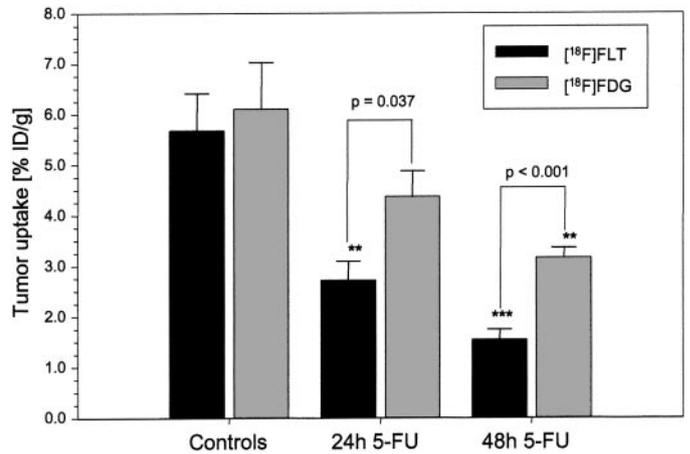TK1 catalytic activity is likely to follow the same pattern as TK1

Fig. 3. 5-FU treatment and tumor [18F]FLT/[18F]FDG uptake. Effect of treatment with 5-FU (165 mg/kg i.p.) on [18F]FLT and [18F]FDG uptake into RIF-1 tumors ($n = 8$–12 mice/group). **, $P < 0.01$, ***, $P < 0.001$, as tested against the control group. Tumors were excised at 60 min after radiotracer injection and their radioactivities were determined by gamma counting as described in the "Materials and Methods" section.

protein levels if ATP levels remained relatively similar. The bioluminescence assay showed that this was not the case. A statistically significant stepwise reduction in tumor ATP levels occurred after treatment with 5-FU compared with untreated controls ($P < 0.001$, one-factorial ANOVA; Fig. 2*C*). Whereas the pretreatment tumor ATP content was 32.8 ± 1.0 μg/mg protein, ATP levels were 27.0 ± 1.0 and 21.5 ± 0.6 μg/mg protein, respectively, at 24 and 48 h after 5-FU treatment.

Biodistribution of [18F]FLT and [18F]FDG. Table 1 summarizes the results of the [18F]FLT and [18F]FDG biodistribution studies in untreated mice. Compared with [18F]FDG, the accumulation of [18F]FLT was significantly higher in blood, plasma, liver, kidneys, and small intestine and significantly lower in brain, spinal cord, heart, and muscle (Table 1). In the untreated tumors, radiotracer uptake appeared to be higher in the [18F]FDG group compared with the [18F]FLT group, but this difference did not reach statistical significance (Fig. 3).

Tumor Radiotracer Uptake in Control and Treated Mice and Correlation with Independent Measures of Treatment Response. Treatment with 5-FU resulted in a stepwise decrease in tumor radiotracer uptake for both the [18F]FLT and [18F]FDG groups. However,

Table 1 *Biodistribution of [18F]FLT and [18F]FDG in untreated RIF-1 tumor-bearing mice[a]*

	[18F]FLT [%ID/g]	[18F]FDG [%ID/g]	P
Tumor	5.7 ± 0.8	6.1 ± 0.9	n.s.
Blood	3.1 ± 0.6	0.4 ± 0.1	0.013
Plasma	3.3 ± 0.7	0.4 ± 0.1	0.006
Liver	3.2 ± 0.8	0.9 ± 0.1	0.029
Kidney	8.3 ± 1.4	2.3 ± 0.6	0.001
Lung	3.9 ± 0.5	4.2 ± 0.5	n.s.
Brain	0.6 ± 0.1	8.1 ± 0.2	<0.001
Urine	454.4 ± 58.2	307.8 ± 23.7	n.s.
Spinal cord	0.7 ± 0.1	5.7 ± 0.3	<0.001
Spleen	7.0 ± 2.3	2.5 ± 0.1	n.s.
Heart	2.9 ± 0.6	44.0 ± 8.9	<0.001
Muscle (leg)	2.7 ± 0.6	5.3 ± 0.8	0.029
Bone (leg)	4.5 ± 1.3	3.0 ± 1.1	n.s.
Small intestine	8.1 ± 1.8	2.2 ± 0.3	0.017

[a] Tissues were excised 1 h after radiotracer administration. Data are mean $\pm$ SE ($n = 8$–12); n.s. = nonsignificant.
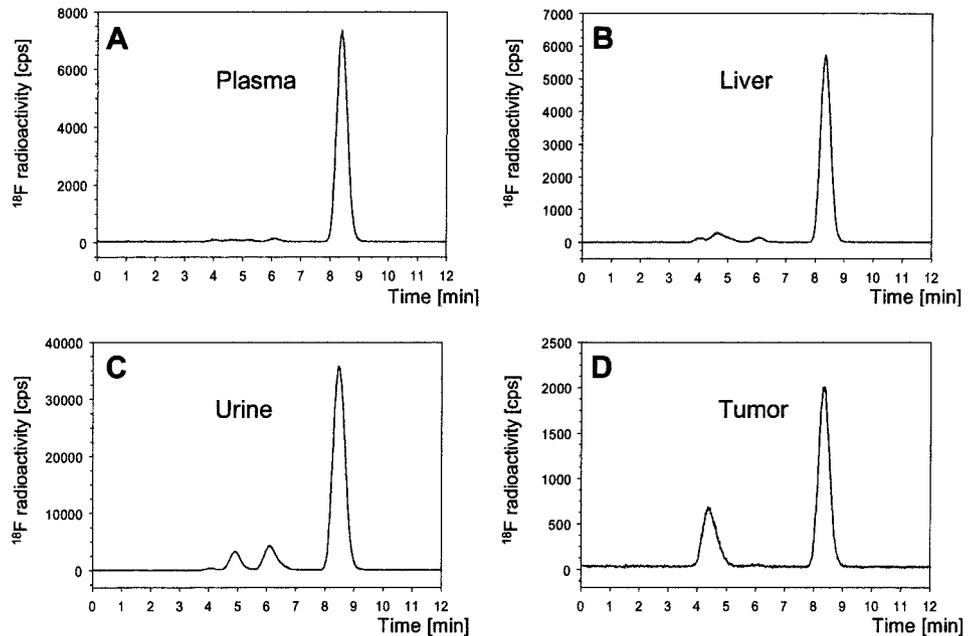
3794

Fig. 4. [18F]FLT metabolism in control mice. Reversed-phase HPLCs of [18F]FLT and putative metabolites in plasma (*A*), liver (*B*), urine (*C*), and untreated RIF-1 tumors (*D*). Samples were obtained 1 h after the radiotracer injection. One main radioactive component at a retention time of 8.5 min, representing the intact [18F]FLT, was observed.

compared with the tumor [18F]FDG uptake, there was a more pronounced decrease in [18F]FLT uptake at 24 h (52.2 ± 7.6 *versus* 28.4 ± 3.3%; $P = 0.037$) and 48 h after 5-FU treatment (72.9 ± 9.9 *versus* 48.2 ± 3.0%; $P < 0.001$). There was a statistically significant difference between untreated controls and 5-FU-treated tumors both at 24 and 48 h after treatment in the [18F]FLT group but only at 48 h after treatment in the [18F]FDG group (Fig. 3). We investigated possible associations between [18F]FLT or [18F]FDG tumor uptake and independent measures of response to 5-FU treatment by comparing radiotracer uptake for individual tumors with the respective tumor volume changes or LI_{PCNA} after 5-FU treatment. [18F]FLT uptake in the RIF-1 tumors (untreated and 5-FU-treated combined) positively correlated with tumor volume changes ($r = 0.585$; $P = 0.001$). A similar correlation was found for [18F]FDG ($r = 0.528$; $P = 0.018$). In addition, tumor [18F]FLT uptake positively correlated with LI_{PCNA} ($n = 9$; $r = 0.71$; $P = 0.031$).

[18F]FLT Is Metabolically Stable *in Vivo*. The radiochromatograms of plasma, liver, urine, and untreated RIF-1 tumor samples, which were obtained 1 h after the administration of [18F]FLT, are shown in Fig. 4. In all cases, the major radioactive component, corresponding to parent [18F]FLT, eluted at a retention time of ~8.5 min. In plasma and liver samples, parent [18F]FLT comprised 96 and 90% of the total radioactivity. In the case of urine and tumor samples, however, minor radioactive peaks at retention times of 5 and 6 min (urine) and 4.5 min (tumor) were detected (18 and 29% of total radioactivity, respectively).

We investigated the possibility that the peak at the HPLC retention time of 4.5 min in tumors was a phosphorylated product. In support of our assertion, the radioactive component at this retention time was distinctly lower in 5-FU-treated tumors (48 h after treatment) compared with untreated tumors (4 *versus* 21%; Fig. 5, *A* and *B*). Furthermore, alkaline phosphatase specifically hydrolyzed the same radioactive metabolite in untreated tumors, resulting in an increased proportion of [18F]FLT. Chromatograms of untreated RIF-1 tumors that were incubated with alkaline phosphatase or incubated under similar conditions without the enzyme are shown in Fig. 5, *C* and *D*.

[18F]FLT-PET Imaging. Fig. 6A shows a typical volume rendered image of the late (30–60 min summed) time frame after the injection of [18F]FLT into a RIF-1 tumor-bearing mouse. Transverse (0.5 mm)

slices of 30–60 min summed [18F]FLT-PET images from an untreated and a 5-FU-treated (48 h after treatment) RIF-1 tumor-bearing mouse are illustrated in Fig. 6, *B* and *C*. The PET images were in agreement with the biodistribution data determined by *ex vivo* gamma counting. In this regard, there was high uptake of radioactivity in tumor, kidney and urine (Fig. 6A). Also in agreement with the biodistribution studies was the fact that the tumor uptake of [18F]FLT was lower for the 5-FU-treated mice (Fig. 6C) than for untreated control (Fig. 6B). The tumor TACs (48 h after 5-FU and controls), normalized to injected activity are shown in Fig. 6D. Radiotracer uptake and retention was seen in untreated control tumors. In contrast, 5-FU-treated tumors showed rapid uptake (delivery) but also rapid elimination of [18F]FLT. The fractional retention of [18F]FLT, calculated by dividing the radioactivity at 60 min p.i. (retention) to that at 5 min p.i. (peak of the delivery phase), was significantly lower in the 5-FU-treated tumors compared with control tumors (0.80 ± 0.06 *versus* 1.09 ± 0.01; $P = 0.026$; $n = 3$/group).

DISCUSSION

[18F]FDG is currently the most widely used radiotracer for imaging therapy response in oncology with PET (for overview, see Ref. 33). It is metabolized to [18F]FDG-phosphate and provides information on the expression of glucose transporters and hexokinase activity (34, 35). However, [18F]FDG is not only trapped in tumor cells but also in macrophages, granulation tissues, and necrosis (36, 37). Therefore, inflammatory or fibrotic masses can compromise response assessment using this radiotracer. These limitations of [18F]FDG has led to the search for alternative approaches with higher specificity.

In this study, we have evaluated a novel pyrimidine nucleoside, [18F]FLT, as a marker for imaging tumor response to therapy by PET. That radiolabeled pyrimidine nucleosides could be more suitable than [18F]FDG for PET imaging of tumor response to therapy was earlier suggested by Reinhardt *et al.* (38) who compared changes in [18F]FDG uptake into AH109A hepatoma-bearing rats after fractionated radiotherapy with that of [3H]dThd (38). A more pronounced decrease in tumor-to-muscle radioactivity ratios for [3H]dThd was reported (38). These results were corroborated by Shields *et al.* (9) in patients with small cell lung cancer and high-grade sarcoma. In that

3795

Fig. 5. 5-FU/alkaline phosphatase and tumor [18F]FLT metabolism. Metabolism (anabolism) of [18F]FLT in RIF-1 tumors as measured by reversed-phase HPLC. *A*, typical chromatogram of an untreated RIF-1 tumor. *B*, typical chromatogram of a 5-FU-treated tumor (165 mg/kg i.p., 48 h after treatment). *C*, typical chromatogram of an untreated RIF-1 tumor after 60 min incubation in buffer. *D*, typical chromatogram of an untreated RIF-1 tumor after 60 min incubation in buffer containing alkaline phosphatase (AP). The metabolite eluting at a retention time of 4.5 min was lower in 5-FU-treated tumors compared with controls. After incubation with alkaline phosphatase, a distinct decrease of the radioactive component at 4.5 min (phosphorylated metabolite) was detected.
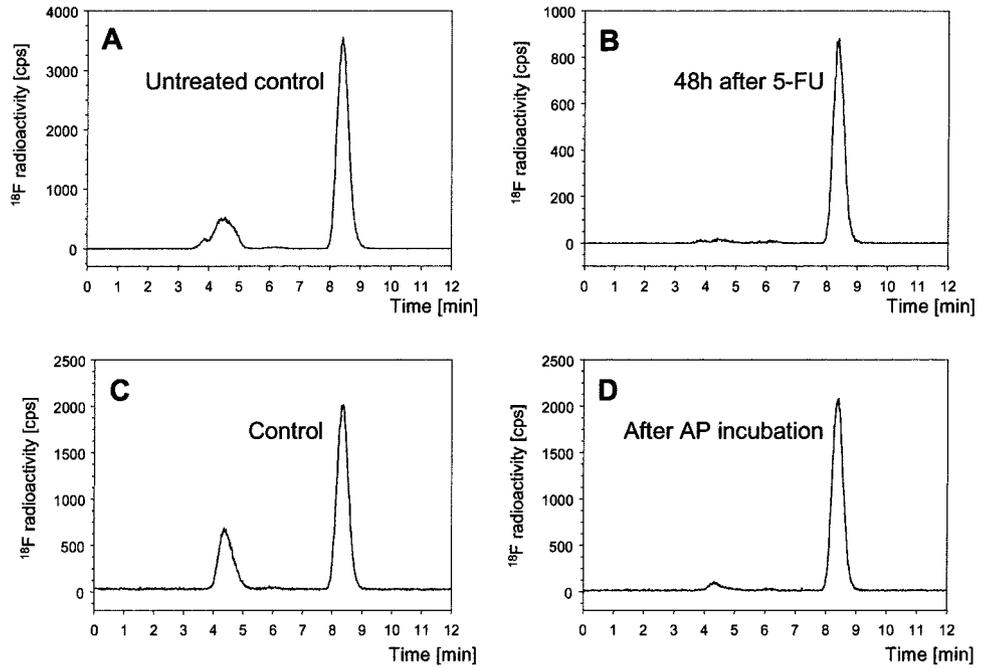
study, the decrease in [11C]dThd uptake at 1 week after chemotherapy was more pronounced than the corresponding decrease in [18F]FDG uptake (9). We have similarly demonstrated in this study an early decrease of [18F]FLT uptake into the RIF-1 tumors after 5-FU treatment, which was more pronounced than that of [18F]FDG. This observation provides additional support for the assertion that imaging tumor proliferation could be more sensitive for response assessment than imaging tumor glucose consumption.

Compared with the gold standard for PET imaging of tumor proliferation, [11C]dThd, [18F]FLT has a number of principal advantages. Firstly, the physical half-life of [18F]FLT is considerably longer (109.4 *versus* 20.4 min). Secondly, [18F]FLT is more stable against

metabolic degradation *in vivo*. This property of [18F]FLT was demonstrated in our mouse model through the finding of very low levels of [18F]FLT metabolites in plasma, liver, and urine. However, preliminary reports in abstract form and images of [18F]FLT have indicated that this radiotracer is metabolized in humans, especially in the liver (12, 39), albeit to a much lesser extent than [11C]dThd (40). The difference in [18F]FLT metabolism between the mouse and humans is presumably because of interspecies differences in expression of UDP-glucuronosyltransferases (41) and may, therefore, limit the usefulness of [18F]FLT for investigating human liver malignancies. Finally, in contrast to [11C]dThd, which is readily incorporated into DNA (42), [18F]FLT is predominantly trapped within the cell as the monophos-
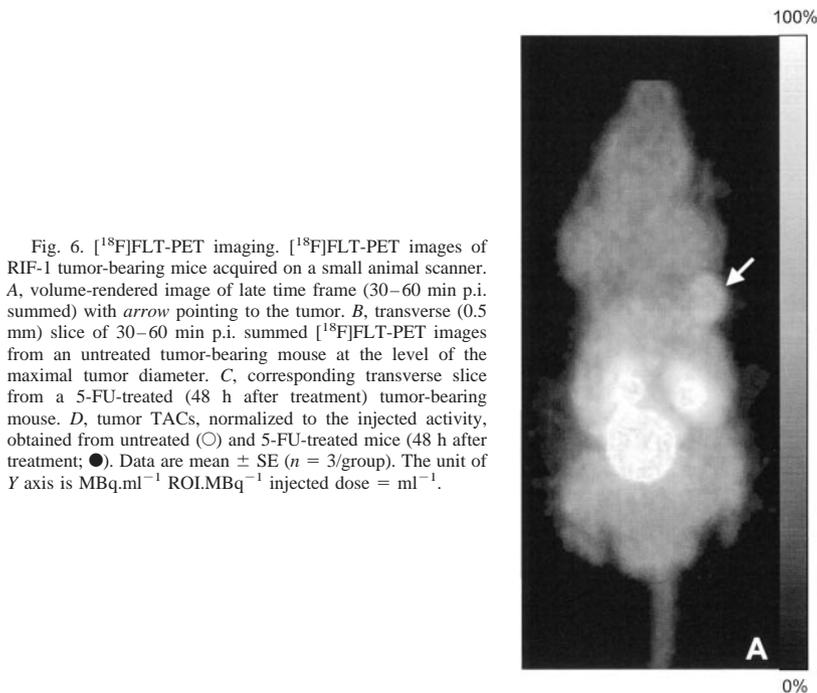

Fig. 6. [18F]FLT-PET imaging. [18F]FLT-PET images of RIF-1 tumor-bearing mice acquired on a small animal scanner. *A*, volume-rendered image of late time frame (30–60 min p.i. summed) with *arrow* pointing to the tumor. *B*, transverse (0.5 mm) slice of 30–60 min p.i. summed [18F]FLT-PET images from an untreated tumor-bearing mouse at the level of the maximal tumor diameter. *C*, corresponding transverse slice from a 5-FU-treated (48 h after treatment) tumor-bearing mouse. *D*, tumor TACs, normalized to the injected activity, obtained from untreated (○) and 5-FU-treated mice (48 h after treatment; ●). Data are mean ± SE (*n* = 3/group). The unit of *Y* axis is MBq.ml^{-1} ROI.MBq^{-1} injected dose = ml^{-1}.

3796
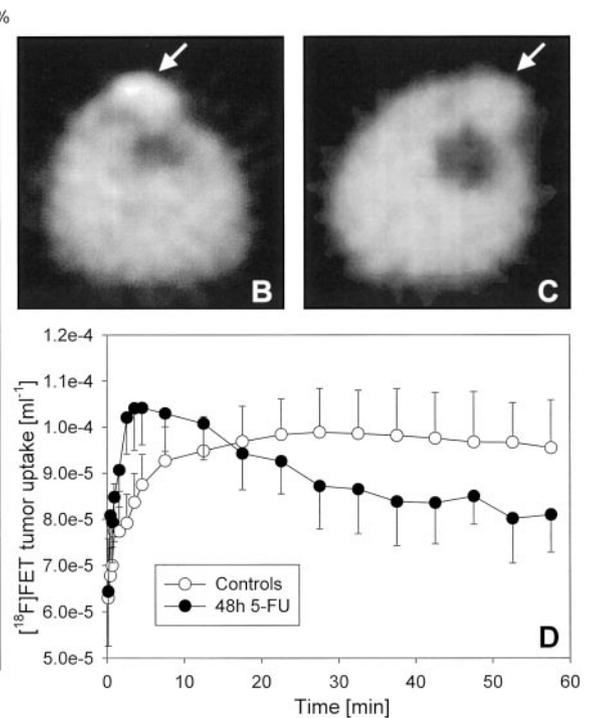
phate (42, 43). Our studies demonstrated the existence of a metabolite in untreated RIF-1 tumors that was identified, biochemically, as a phosphate anabolite of [18F]FLT. Treatment of RIF-1 tumors with 5-FU decreased [18F]FLT phosphorylation, an important finding in the use of [18F]FLT for response assessment.

To date, only one preliminary report has described the use of [18F]FLT-PET for *in vivo* monitoring tumor response to anticancer therapy (44). In that study, two patients with primary breast cancer were imaged before and after neoadjuvant chemotherapy. A decrease of the [18F]FLT tumor uptake by 21 and 83% was detected after the first course of the chemotherapy, with complete normalization of [18F]FLT uptake after completion of therapy (44). In our model system, there was a stepwise decrease of tumor [18F]FLT uptake to 48 and 27% of that of untreated control tumors at 24 and 48 h after 5-FU treatment, respectively. In addition, the PET imaging studies showed that the fractional retention of [18F]FLT was lower at 48 h after 5-FU treatment compared with control tumors. This parameter may, therefore, be applicable to the analysis of clinical [18F]FLT data. The higher initial [18F]FLT delivery into the 5-FU-treated tumors could be attributed to increased tumor blood flow, which is characteristic of 5-FU-treated RIF-1 tumors (45). Compared with *ex vivo* gamma counting, PET imaging was less efficient in discriminating between treated and control tumors at 60 min. This could be attributed to partial volume and spill over effects, which are more pronounced in the imaging of small animals, as well as the use of anesthesia in the imaging studies (decreasing [18F]FLT clearance).

FLT is a substrate for cytoplasmic TK1 (18). The rationale for using [18F]FLT-PET in measuring the proliferative activity of tumors is based on the S-phase-specific induction of TK1 at the transcriptional and posttranscriptional level (46). TK1 is nearly undetectable in growth-arrested cells but dramatically stimulated at the G_1-S border (46, 47). The sequences responsible for the S-phase-specific expression of TK1 have been mapped to promotor regions that carry binding sites for transcription factors of the E2F and Sp1 families (48, 49). The stability of TK1 dramatically decreases upon cell division, resulting in the rapid clearance of the enzyme from newly divided G_1 cells (46). Accordingly, two recent reports showed positive correlations between FLT uptake and percentage of S-phase fraction *in vitro* in different tumor cell lines (18, 42).

In our study, we demonstrated an initial decrease in TK1 protein concentration at 24 h after 5-FU treatment. At the later time point (48 h after treatment), however, an intense increase in TK1 protein levels was detected. The increased TK1 protein expression (reproducible in three separate 5-FU treatment experiments) was unexpected given the stepwise reduction of [18F]FLT uptake after treatment. Thus, we evaluated the levels of the other factor that contributes to TK1 activity, the cofactor ATP. Munch-Petersen *et al.* (20) first described ATP as an important cofactor for realizing the activity of TK1. In their experiments with TK1 purified from human phytohemagglutinin-stimulated lymphocytes, the activity of the enzyme in the presence of ATP was shown to be more than twice as high as the activity of TK1 without ATP (20). This finding was explained by a reversible, ATP-dependent effect on the enzyme size, transforming TK1 to a dimer in the absence and to a tetramer in the presence of ATP, with higher K_m and lower k_{cat} values for the dimer (20). In our model system, ATP levels in the 5-FU-treated tumors were significantly lower than those in untreated control tumors. Taken together, the decrease in tumor [18F]FLT uptake at 48 h after treatment despite increased TK1 protein expression at that time point could be explained by the decrease in ATP levels, *i.e.,* changes in catalytic activity but not changes in translation or posttranslation stability. This effect may be specific for 5-FU and other thymidylate synthase inhibitors. For other anticancer drugs, especially those that target cell cycle control, we would spec-

ulate that a decrease in [18F]FLT uptake will ensue from a decrease in TK1 protein levels.

[18F]FLT uptake was validated by comparison to PCNA labeling, an established measure of proliferation. PCNA is a M_r 36,000, acidic, nonhistone, nuclear protein in which the expression is associated with the late G_1 and S-phase of the cell cycle (50, 51). A positive correlation was found between tumor [18F]FLT uptake and LI_{PCNA}, supporting the value of [18F]FLT for assessing antiproliferative activity of 5-FU. The posttreatment tumor [18F]FLT uptake was also associated with changes in tumor volume, a parameter that—in approximation—represents the current gold standard for clinical evaluation of antitumor therapy obtained by anatomical imaging methods like ultrasound, X-ray transmission computed tomography, and magnetic resonance imaging. Given the biochemical basis of [18F]FLT uptake, it is possible that [18F]FLT-PET could be used to detect response not only to cytotoxic but also to cytostatic agents.

In conclusion, using a RIF-1 tumor model, we have shown an association between tumor [18F]FLT uptake in biodistribution studies and proliferation. Changes in tumor [18F]FLT accumulation after 5-FU treatment were successfully imaged by PET. These changes reflect established measures of tumor response. In addition, our study provides additional support for the presumption that TK1 catalytic activity is important for [18F]FLT uptake: in our model system, the decrease in TK1 activity after 5-FU treatment was not explained by decreased TK1 protein levels but by a decrease in cofactor ATP levels. Compared with [18F]FDG, the decrease of tumor radiotracer accumulation in response to antiproliferative treatment was more pronounced for [18F]FLT. [18F]FLT is, therefore, a promising marker and warrants additional preclinical and clinical testing.

ACKNOWLEDGMENTS

REFERENCES

1. Pommier, Y., Pourquier, P., Urasaki, Y., Wu, J., and Laco, G. S. Topoisomerase I inhibitors: selectivity and cellular resistance. Drug Resist. Updat., *2:* 307–318, 1999.
2. Owa, T., Yoshino, H., Yoshimatsu, K., and Nagasu, T. Cell cycle regulation in the G_1 phase: a promising target for the development of new chemotherapeutic anticancer agents. Curr. Med. Chem., *8:* 1487–1503, 2001.
3. Matter, A. Tumor angiogenesis as a therapeutic target. Drug Discov. Today, *6:* 1005–1024, 2001.
4. Therasse, P., Arbuck, S. G., Eisenhauer, E. A., Wanders, J., Kaplan, R. S., Rubinstein, L., Verweij, J., Van Glabbeke, M., van Oosterom, A. T., Christian, M. C., and Gwyther, S. G. New guidelines to evaluate the response to treatment in solid tumors. J. Natl. Cancer Inst. (Bethesda), *92:* 205–216, 2000.
5. Padhani, A. R., and Husband, J. E. Are current tumor response criteria relevant for the 21st century? Br. J. Radiol., *73:* 1031–1033, 2000.
6. Sundoro-Wu, B. M., Schmall, B., Conti, P. S., Dahl, J. R., Drumm, P., and Jacobsen, J. K. Selective alkylation of pyrimidyldianions: synthesis and purification of 11C labeled thymidine for tumor visualization using positron emission tomography. Int. J. Appl. Radiat. Isot., *35:* 705–708, 1984.
7. Martiat, P., Ferrant, A., Labar, D., Cogneau, M., Bol, A., Michel, C., Michaux, J. L., and Sokal, G. *In vivo* measurement of carbon-11 thymidine uptake in non-Hodgkin's lymphoma using positron emission tomography. J. Nucl. Med., *29:* 1633–1637, 1988.
8. Eary, J. F., Mankoff, D. A., Spence, A. M., Berger, M. S., Olshen, A., Link, J. M., O'Sullivan, F., and Krohn, K. A. 2-[C-11]Thymidine imaging of malignant brain tumors. Cancer Res., *59:* 615–621, 1999.
9. Shields, A. F., Mankoff, D. A., Link, J. M., Graham, M. M., Eary, J. F., Kozawa, S. M., Zheng, M., Lewellen, B., Lewellen, T. K., Grierson, J. R., and Krohn, K. A. Carbon-11-thymidine and FDG to measure therapy response. J. Nucl. Med., *39:* 1757–1762, 1998.
10. Eary, J. F., Mankoff, D. A., Thompson, J. A., Gold, P., and Krohn, K. A. Tumor metabolism and proliferation using quantitative PET imaging in renal cell carcinoma patients treated with IL-2. Proc. Am. Soc. Clin. Oncol. Annu. Meet., *13* (Suppl.)*:* 338a, 1999.
11. Wells, P., Gunn, R. N., Alison, M., Steel, C., Golding, M., Ranicar, A. S., Brady, F., Osman, S., Jones, T., and Price, P. Assessment of proliferation *in vivo* using

2-[(11)C]thymidine positron emission tomography in advanced intra-abdominal malignancies. Cancer Res., *62:* 5698–5702, 2002.

12. Shields, A. F., Grierson, J. R., Dohmen, B. M., Machulla, H. J., Stayanoff, J. C., Lawhorn-Crews, J. M., Obradovich, J. E., Muzik, O., and Mangner, T. J. Imaging proliferation *in vivo* with [¹⁸F]FLT and positron emission tomography. Nat. Med., *4:* 1334–1336, 1998.

13. Schields, A. F., Ho, P. T., and Grierson, J. R. The role of imaging in the development of oncological agents. J. Clin. Pharmacol., *39:* 40–44, 1999.

14. Langen, P., Etzold, G., Hintsche, R., and Kowollik, G. 3′-Deoxy-3′-fluorothymidine, a new selective inhibitor of DNA-synthesis. Acta Biol. Med. Ger., *23:* 759–766, 1969.

15. Flexner, C., van der Horst, C., Jacobson, M. A., Powderly, W., Duncanson, F., Ganes, D., Barditch-Crovo, P. A., Petty, B. G., Baron, P. A., and Armstrong, D. Relationship between plasma concentration of 3′-deoxy-3′-fluorothymidine (alovudine) and anti-retroviral activity in two concentration-controlled trials. J. Infect. Dis., *170:* 1394–1403, 1994.

16. Sundseth, R., Joyner, S. S., Moore, J. T., Dornsife, R. E., and Dev, I. K. The anti-human immunodeficiency virus agent 3′-fluorothymidine induced DNA damage and apoptosis in human lymphoblastoid cells. Antimicrob. Agents Chemother., *40:* 331–335, 1996.

17. Kong, X. B., Zhu, Q. Y., Vidal, P. M., Watanabe, K. A., Polsky, B., Armstrong, D., Ostrander, M., Lang, S. A., Jr., Muchmore, E., and Chou, T. C. Comparison of anti-human immunodeficiency virus activities, cellular transport, and plasma and intracellular pharmacokinetics of 3′-fluoro-3′-deoxythymidine and 3′-azido-3′-deoxythymidine. Antimicrob, Agents Chemother., *36:* 808–818, 1992.

18. Rasey, J. S., Grierson, J. R., Wiens, L. W., Kolb, P. D., and Schwartz, J. L. Validation of FLT uptake as a measure of thymidine kinase-1 activity in A549 carcinoma cells. J. Nucl. Med., *43:* 1210–1217, 2002.

19. Ellims, P. H., Van der Weyden, M. B., and Medley, G. Thymidine kinase isoenzymes in human malignant lymphoma. Cancer Res., *41:* 691–695, 1981.

20. Munch-Petersen, B., Cloos, L., Jensen, H. K., and Tyrsted, G. Human thymidine kinase. I. Regulation in normal and malignant cells. Adv. Enzyme Regul., *35:* 69–89, 1995.

21. Sherley, J. L., and Kelly, T. J. Regulation of human thymidine kinase during the cell cycle. J. Biol. Chem., *263:* 8350–8358, 1988.

22. Wilson, I. K., Chatterjee, S., and Wolf, W. The use of 3′-fluoro-3′-deoxythymidine and studies of its ¹⁸F-labelling, as a tracer for the non-invasive monitoring of the biodistribution of drugs against AIDS. J. Fluorine Chem., *55:* 283–289, 1991.

23. Grierson, J. R., Shields, A. F., and Eary, J. F. Development of a radiosynthesis for 3′-[F-18]fluoro-3′-deoxynucleosides. J. Labelled Compounds Radiopharm., *40:* 60–62, 1997.

24. Mier, W., Haberkorn, U., and Eisenhut, M. [¹⁸F]FLT; portrait of a proliferation marker. Eur. J. Nucl. Med. Mol. Imag., *29:* 165–169, 2001.

25. Buck, A. K., Schirrmeister, H., Hetzel, M., Von Der Heide, M., Halter, G., Glatting, G., Mattfeldt, T., Liewald, F., Reske, S. N., and Neumaier, B. 3-Deoxy-3-[(18)F]fluorothymidine-positron emission tomography for noninvasive assessment of proliferation in pulmonary nodules. Cancer Res., *62:* 3331–3334, 2002.

26. Aboagye, E. O., Bhujawala, Z. M., Shungu, D. C., and Glickson, J. D. Detection of tumor response to chemotherapy by ¹H nuclear magnetic resonance spectroscopy: effect of 5-fluorouracil on lactate levels in radiation-induced fibrosarcoma 1 tumors. Cancer Res., *58:* 1063–1067, 1998.

27. Moore, M. J., and Erlichmann, C. Pharmacology of anticancer drugs. *In:* I. F. Tannock and R. P. Hill (eds.), The Basic Science of Oncology, pp. 370–391. New York: McGraw-Hill, 1998.

28. Cleij, M. C., Steel, C. J., Brady, F., Ell, P. J., Pike, V. W., and Luthra, S. K. An improved synthesis of 3′-deoxy-3′-[¹⁸F]fluorothymidine ([¹⁸F]FLT) and the fate of the precursor 2,3′-anhydro-5′-O-(4,4′-dimethoxytrityl)-thymidine. J. Labelled Compounds Radiopharm., *44* (Suppl. 1)*:* 871–873, 2001.

29. Hamacher, K., Coenen, H. H., and Stöcklin, G. Efficient stereospecific synthesis of no-carrier-added 2-[¹⁸F]-fluoro-2-deoxy-D-glucose using aminopolyether supported nucleophilic substitution. J. Nucl. Med., *27:* 235–238, 1986.

30. He, Q., Skog, S., Wang, N., Eriksson, S., and Tribukait, B. Characterization of a peptide antibody against a C-terminal part of human and mouse cytosolic thymidine kinase, which is a marker of cell proliferation. Eur. J. Cell Biol., *70:* 117–124, 1996.

31. He, Q., Zou, L., Zhang, P. A., Lui, J. X., Skog, S., and Fornander, T. The clinical significance of thymidine kinase 1 measurement in serum of breast cancer patients using anti-TK1 antibody. Int. J. Biol. Markers, *15:* 139–146, 2000.

32. Jeavons, A. P., Chandler, R. A., and Dettmat, C. A. A 3D HIDAC-PET camera with sub-millimetre resolution for imaging small animals. IEEE Trans. Nucl. Sci., *46:* 468–473, 1999.

33. Young, H., Baum, R., Cremerius, U., Herholz, K., Hoekstra, O., Lammertsma, A. A., Pruim, J., and Price, P. Measurement of clinical and subclinical tumour response using [¹⁸F]-fluorodeoxyglucose and positron emission tomography: review and 1999 EORTC recommendations. Eur. J. Cancer, *35:* 1773–1782, 1999.

34. Hatanaka, M., Augl, C., and Gilden, R. V. Evidence for a functional change in the plasma membrane of murine sarcoma virus-infected mouse embryo cells. Transport and transport-associated phosphorylation of 14C-2-deoxy-D-glucose. J. Biol. Chem., *245:* 714–717, 1970.

35. Gallagher, B. M., Fowler, J. S., Gutterson, N. I., MacGregor, R. R., Wan, C. N., and Wolf, A. P. Metabolic trapping as a principle of radiopharmaceutical design: some factors responsible for the biodistribution of [18F] 2-deoxy-2-fluoro-D-glucose. J. Nucl. Med., *19:* 1154–1161, 1978.

36. Kubota, R., Yamada, S., Kubota, K., Ishiwata, K., Tamahashi, N., and Ido, T. Intratumoral distribution of 18F-fluorodeoxyglucose *in vivo*: high accumulation in macrophages and granulation tissues studied by microautoradiography. J. Nucl. Med., *33:* 1972–1980, 1992.

37. Kubota, R., Kubota, K., Yamada, S., Tada, M., Ido, T., and Tamahashi, N. Active and passive mechanisms of [fluorine-18] fluorodeoxyglucose uptake by proliferating and prenecrotic cancer cells *in vivo*: a microautoradiographic study. J. Nucl. Med., *35:* 1067–1075, 1994.

38. Reinhardt, M. J., Kubota, K., Yamada, S., Iwata, R., and Yagashi, H. Assessment of cancer recurrence in residual tumors after fractionated radiotherapy: a comparison of fluorodeoxyglucose, L-methionine and thymidine. J. Nucl. Med., *38:* 280–287, 1997.

39. Shields, A. F., Dohmen, B. M., Mangner, T. J., Kuntzsch, M., Bares, R., Stayanoff, J, Muzik, O., and Machulla, H. J. Metabolism of ¹⁸F-FLT in patients. J. Nucl. Med., *41* (5 Suppl.)*:* 36p, 2000.

40. Conti, P. S., Hilton, J., Wong, D. F., Alauddin, M. M., Dannals, R. F., Ravert, H. T., Wilson, A. A., and Anderson, J. H. High performance liquid chromatography on carbon-11 labeled thymidine and its major catabolites for clinical PET studies. Nucl. Med. Biol., *21:* 1045–1051, 1994.

41. Court, M. H. Acetaminophen UPD-glucuronosyltransferase in ferrets: species and gender differences, and sequence analysis of ferret UGT1A6. J Vet Pharmacol. Ther., *24:* 415–422, 2001.

42. Toyohara, J., Waki, A., Takamatsu, S., Yonekura, Y., Magata, Y., and Fujibayashi, Y. Basis of FLT as a cell proliferation marker: comparative studies with [³H]thymidine and [³H]arabinothymidine, and cell-analysis in 22 asynchronously growing tumor cell lines. Nucl. Med. Biol., *29:* 281–287, 2002.

43. Seitz, U., Wagner, M., Neumaier, B., Wawra, E., Glatting, G., Leder, G., Schmid, R. M., and Reske, S. N. Evaluation of pyridine metabolising enzymes and *in vitro* uptake of 3′-[¹⁸F]fluoro-3′-deoxythymidine ([¹⁸F]FLT) in pancreatic cancer cell lines. Eur. J. Nucl. Med. Mol. Imag., *29:* 1174–1181, 2002.

44. Dohmen, B. M., Shields, A. F., Dittmann, H., Fersis, N., Eschmann, S. M., Philip, P., Reimold, M., Machulla, H. J., and Bares, R. Use of [¹⁸F]FLT for breast cancer imaging. J. Nucl. Med., *42* (Suppl.)*:* 29, 2001.

45. Li, S. J., Wehrle, J. P., Glickson, J. D., Kumar, N., and Braunschweiger, P. G. Tumor bioenergetics and blood flow in RIF-1 murine tumors treated with 5-fluorouracil. Magn. Reson. Med., *22:* 47–56, 1991.

46. Sherley, J. L., and Kelly, T. J. Regulation of human thymidine kinase during the cell cycle. J. Biol. Chem., *262:* 8350–8358, 1988.

47. Sutterluety, H., Bartl, S., Dötzlhofer, A., Khier, H., Wintersberger, E., and Seiser, C. Growth-regulated antisense transcription of the mouse thymidine kinase gene. Nucleic Acids Res., *26:* 4989–4995, 1998.

48. Tommasi, S., and Pfeifer, G. P. Constitutive protection of E2F recognition sequences in the human thymidine kinase promotor during cell cycle progression. J. Biol. Chem., *272:* 30483–30490, 1997.

49. Sorensen, P., and Wintersberger, E. Sp1 and NF-Y are necessary and sufficient for growth-dependent regulation of the hamster thymidine kinase promotor. J. Biol. Chem., *274:* 30943–30949 1999.

50. Celis, J. E., and Celis, A. Cell cycle-dependent variations of the distribution of the nuclear protein cyclin proliferating cell nuclear antigen in cultured cells: subdivision of S phase. Proc. Natl. Acad. Sci. USA, *82:* 3262–3266, 1985.

51. Mathews, M. B., Bernstein, R. M., Franza, B. R., Jr., and Garrels, J. I. Identity of the proliferating cell nuclear antigen and cyclin. Nature (Lond.), *309:* 374–376, 1984.

3′-Deoxy-3′-[18F]Fluorothymidine as a New Marker for Monitoring Tumor Response to Antiproliferative Therapy *in Vivo* with Positron Emission Tomography

Henryk Barthel, Marcel C. Cleij, David R. Collingridge, et al.

Updated version	Access the most recent version of this article at: http://cancerres.aacrjournals.org/content/63/13/3791

Cited articles	This article cites 50 articles, 20 of which you can access for free at: http://cancerres.aacrjournals.org/content/63/13/3791.full#ref-list-1
Citing articles	This article has been cited by 54 HighWire-hosted articles. Access the articles at: http://cancerres.aacrjournals.org/content/63/13/3791.full#related-urls

E-mail alerts	Sign up to receive free email-alerts related to this article or journal.
Reprints and Subscriptions	To order reprints of this article or to subscribe to the journal, contact the AACR Publications Department at pubs@aacr.org.
Permissions	To request permission to re-use all or part of this article, use this link http://cancerres.aacrjournals.org/content/63/13/3791. Click on "Request Permissions" which will take you to the Copyright Clearance Center's (CCC) Rightslink site.